Energy Materials

Review

Fluorine chemistry in lithium-ion and sodium-ion batteries

Zibing Pan[1], Huaqi Chen[1], Yubin Zeng[1], Yan Ding[2], Xiangjun Pu[2,*], Zhongxue Chen[1,*] (iD)

[1]Key Laboratory of Hydraulic Machinery Transients, Ministry of Education, School of Power and Mechanical Engineering, Wuhan University, Wuhan 430072, Hubei, China.
[2]Hubei Key Laboratory of Electrochemical Power Sources, College of Chemistry and Molecular Sciences, Wuhan University, Wuhan 430072, Hubei, China.

*Correspondence to: Prof./Dr. Zhongxue Chen, Key Laboratory of Hydraulic Machinery Transients, Ministry of Education, School of Power and Mechanical Engineering, Wuhan University, No. 299 Bayi Road, Wuchang District, Wuhan 430072, Hubei, China.
E-mail: zxchen_pmc@whu.edu.cn; Dr. Xiangjun Pu, Hubei Key Laboratory of Electrochemical Power Sources, College of Chemistry and Molecular Sciences, Wuhan University, No.299 Bayi Road, Wuchang District, Wuhan 430072, Hubei, China.
E-mail: joy_pu@whu.edu.cn

Abstract

As the peculiar element in the Periodic Table of Elements, fluorine gas owns the highest standard electrode potential of 2.87 V *vs.* F⁻, and a fluorine atom has the maximum electronegativity. Benefiting from the prominent property, fluorine plays an important role in the development of lithium-ion batteries (LIBs) and sodium-ion batteries (SIBs) in terms of cathode materials (transition metal fluorides, fluorinated polyanionic compounds), electrolytes, and interfaces. In cathode materials, the highly electronegative renders enhanced ionic character of transition metal fluorine bonds and correspondingly high working potential in electrolytes; fluorinated electrolytes possess good antioxidant ability and flame retardance, which can significantly improve the thermal safety of a battery. On an electrode-electrolyte interface, the fluorine-rich inorganic component (such as LiF and NaF) is essential for the formation of a robust and stable solid electrolyte interface on anodes. Despite the remarkable advances achieved in fluorinated cathodes, electrolytes, and interfaces, there is still a lack of comprehensive understanding of the function of fluorides in LIBs and SIBs. Accordingly, this review briefly summarized the recent progress of fluorine-based electrodes, electrolytes, and interfaces and highlighted the correlation between the composition, property, and function to reveal the fluorine chemistry in LIBs and SIBs. This review will provide guidance for the rational design and targeted regulation of fluorine-dominated high-performance electrode materials, functionalized electrolytes, and consolidated interfaces.

Keywords: Fluorine chemistry, lithium/sodium ion batteries, cathode materials, electrolytes, interfaces

INTRODUCTION

As major challenges facing humanity, climate change and exhaustion of fossil fuels today are facilitating the development of renewable resources such as wind and solar energy[1]. However, the intermittent nature of these renewable energies could only generate electricity under favorable circumstances. In recent years, there has been a significant focus on the development of multiscale electrochemical energy storage systems (EESSs) based on rechargeable batteries. This approach aims to address the increasing energy demand while maximizing the utilization of sustainable energy sources.

Lithium/sodium ion batteries (LIBs/SIBs) consist of four parts: cathodes, anodes, separators, and electrolytes. Li^+/Na^+ ions are inserted/extracted between the cathode/anode by the electrolyte to store or release energy. Fluorine plays an important role in the electrode, electrolyte, and electrode-electrolyte interface (EEI) of LIBs and SIBs. As the most electronegative element, fluorine atoms have a strong tendency to accept electrons, which allows the introduction of fluorine into the electrode to bring the advantages of high voltage and high energy density to the battery. Fluorinated electrodes, such as CuF_2 and CoF_3 cathodes, were studied early in the development of lithium batteries[2]. These materials adopting combined insertion-conversion type reactions were studied for space-oriented lithium batteries. Later, FeF_3, a cheap and high-capacity cathode material, was further reported by Arai *et al.* The other fluorine-involved cathodes are fluorine-substituted polyanionic compounds[3]. Vanadium fluorine phosphates, $LiVPO_4F$ and $NaVPO_4F$, were first reported by Baker in 2003[4]. This discovery paved the way for the exploration and development of various derivative materials for LIBs and SIBs, including $LiFeSO_4F$, $NaFeSO_4F$[5], $Na_{0.5}VPO_{4.8}F_{0.7}$[6], *etc*.

In addition to electrodes, it is well recognized that an electrolyte is an indispensable component in any electrochemical device. Numerous pieces of literature in recent years have also verified the pivotal role of fluorine in electrolytes. As to electrolytes, fluorinated electrolytes have two main merits in terms of high voltage stability and forming fluorinated solid electrolyte interphase (SEI)[7]. The former renders electrolytes able to be operated under high voltage, which backs up higher specific energy density. While the latter not only acts as excellent electronic insulators and good ion conductors but also presents high interfacial energy to the anode metal to suppress dendrite, for instance, LiF could promote Li^+ migration along the interface and encourage growth of the deposited Li in a parallel direction[8].

The purpose of this review is to briefly summarize the unique roles of fluorine in battery cathode materials and electrolytes [Figure 1] to provide perspectives and strategies for future design of battery functional with long lifespan, high energy density, high power, and high safety under different application conditions.

The role of fluorine in cathode materials

The voltage trend of transition metal-based cathode materials roughly follows the formal charges of the central atoms in the structure, consisting of the idea of the inductive effect. F has the strongest electronegativity (3.98 on the Pauling scale), thus endowing the metal fluorine (M-F) bond with a high ionic character. The presence of strong M-F bonding stabilizes the antibonding M^{n+}/M^{n+1} state through a M-F inductive effect to generate high operating voltage.

Transitional metal fluoride cathodes

Metal fluorides (denoted as MF_n) are a class of cathode materials that have attracted extensive research interests. These materials have a large specific capacity due to the possibility of multiple electron transfer at a single redox center, such as FeF_3, FeF_2 to Fe^0[9], In LIBs and SIBs, an overall chemical reaction equation is
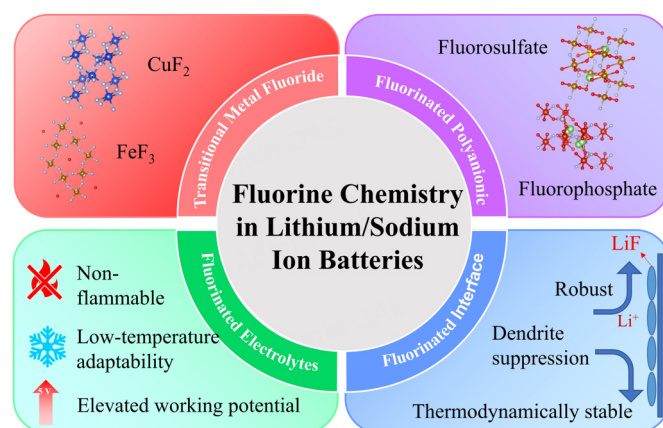
Figure 1. Summary of the role of fluorine in lithium/sodium ion batteries.

given as: $nA^+ + ne^- + MF_n \rightarrow nAF + M$ (A denotes Na or Li, M denotes transition metals such as Fe, Cu, *etc.* if not specified, the same below). Specifically, both insertion and conversion reactions may happen during this progress[10] [Figure 2A]. Simultaneously, metal fluorides typically provide a higher working potential compared to oxides and sulfides as a result of the high electronegativity of fluorine[11] [Figure 2A]. To illustrate, in the case of LIBs, FeF_3 boasts a theoretical potential of 2.74 V (*vs.* Li^+/Li)[12], while Fe_2O_3 displays a lower theoretical potential of 1.63 V (*vs.* Li^+/Li)[13]. This highlights the superior performance of metal fluorides in terms of working potential.

CuF_2 was initially introduced as a cathode material for primary lithium batteries and possesses a high working potential of 3.55 V, which gives it a high energy density of 1,874 Wh kg^{-1}[2]. However, the lithium storage in CuF_2 is irreversible: during the first lithiation process, copper will form large isolated particles when the conversion reaction occurs, which separates Cu from LiF and isolates the electron transport path [Figure 2B][14,15]. Hua *et al.* showed that competition between Cu dissolution and $Cu + 2LiF \rightarrow CuF_2$ reaction occurs during the electrode process due to the presence of a large overpotential, thus consuming the LiF phase formed during discharge[16]. To solve Cu dissolution, the strategy of metal oxide coating was proposed. To improve the reversibility, Seo *et al.* used NiO to coat CuF_2 particles (denoted by CuF_2-NiO/C) as compared to original CuF_2 (denoted by CuF_2/C)[17]. The presence of NiO decreases the interaction between the electrode and the electrolyte, thereby moderating the dissolution of Cu, thus realizing reversible cycling of CuF_2 [Figure 2C]. Another way to improve the reversibility of CuF_2 is to construct a conductive network during its lithiation and enhance the reversibility by forming solid solutions of CuF_2 with other metal fluorides (e.g., FeF_2, NiF_2). Wang *et al.* constructed a ternary metal fluoride material ($Cu_xFe_{1-x}F_2$)[18]. During the first discharge process, Cu^{2+} is first reduced to metallic Cu^0 and forms disordered FeF_2, after which Fe^{2+} is reduced to metallic Fe^0. During the subsequent charging, Fe^0 is reconversion to FeF_2, then Fe partially oxidized to form a rutile-like iron fluoride framework (with Fe at a valence of $Fe^{2+/3+}$), which facilitates the nucleation and growth of Cu fluoride because of their structural similarity [Figure 2D]. The benefit led to an initial discharge capacity of 575 mAh g^{-1}, with the ability to keep the capacity over 450 mAh g^{-1} in subsequent cycles [Figure 2E].

Wang *et al.* have proposed that iron-based metal fluoride forms a bicontinuous iron network during discharge[14], which provides a large LiF/Fe interface area and a highly conductive pathway for local electron transport, thus facilitating the conversion in subsequent cycles. In contrast to FeF_x, the converted product from CuF_2 consists of larger Cu nanoparticles isolated from the LiF phase, which is mainly responsible for the lack of reversibility in CuF_2. To avoid the irreversibility issue of CuF_2, various iron-based metal fluorides
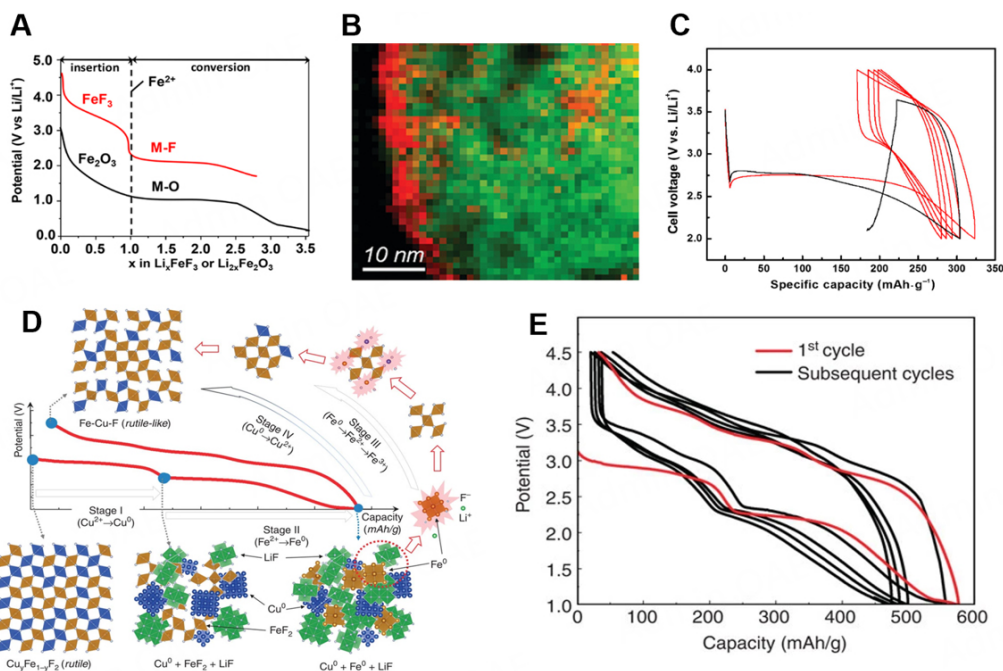
Figure 2. (A) Discharge curves of FeF_3 and Fe_2O_3, which show that metal fluorides have higher operation potential than oxides. This figure is quoted with permission from Lemoine *et al.*[10]. (B) False-color composite image of the converted electrode showing LiF (red) and Cu (green) phases separate from each other. This figure is quoted with permission from Wang *et al.*[14]. (C) Voltage profiles of CuF_2/C (black) and NiO-CuF_2/C (red) electrodes. NiO coating reduces Cu dissolution and improves CuF_2 reversibility. This figure is quoted with permission from Seo *et al.*[17]. (D) Schematic illustration of the asymmetric reaction pathway in $Cu_yFe_{1-y}F_2$. This figure is quoted with permission from Wang *et al.*[18]. (E) Voltage profiles of $Cu_{0.5}Fe_{0.5}F_2$ for the first five cycles at 9.2 mA g^{-1}. This figure is quoted with permission from Wang *et al.*[18].

with much better reversibility have been explored. The ReO_3-type FeF_3 (Figure 3A, the first one) was tested for lithium storage in 1997 with a discharging capacity of 140 mAh g^{-1} for the first week in the voltage range of 4.5-2.5 V (*vs.* Li^+/Li) and then exhibited a capacity of 80 mAh g^{-1} in subsequent cycles[3,19]. Until 2003, Liu *et al.* mechanically milled FeF_3 with different types of carbon to obtain carbon-FeF_3 nanocomposites (FeF_3@C) to improve the electrochemical properties[13]. The material exhibited a reversible capacity of 600 mAh g^{-1} at 70 °C. They also found another reversible plateau at 2 V, exhibiting a discharge specific capacity of 367 mAh g^{-1}. Through *in-situ* and *ex-situ* XRD analysis, the following reaction mechanisms were proposed:

$$Li^+ + 1\ e^- + Fe^{III}F_3 \rightarrow LiFe^{II}F_3\ (4.5\text{-}2.5\ V\ vs.\ Li^+/Li)$$

$$LiFe^{II}F_3 + 2Li \rightarrow 3LiF + Fe^0\ (2.5\text{-}1.5\ V\ vs.\ Li^+/Li)$$
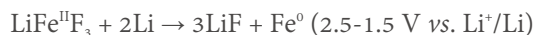
Despite the fact that FeF_3 exhibits attractive lithium storage properties, it shows severe polarization and sluggish kinetics during cycling[20]. Considerable efforts have been undertaken to comprehend the mechanism and, hence, mitigate these issues. Through *in-situ* X-ray absorption spectroscopy, *in-situ* transmission electron microscopy, and density functional theory (DFT) calculations, Li *et al.* proposed a new reaction mechanism: $FeF_3 \rightarrow Li_{0.25}FeF_3 \leftrightarrow LiF + FeF_2 \leftrightarrow Fe + 3LiF$ [Figure 3B][21]. In this process, the uneven distribution of the electrochemically active phases brought about a serious ohmic voltage drop. To further, Hua *et al.* found that FeF_3 undergoes a three-phase reaction upon Li^+ insertion, generating a small amount of FeF_2 through a replacement-like mechanism[22]. During the deeper lithiation process, Fe^{3+} is
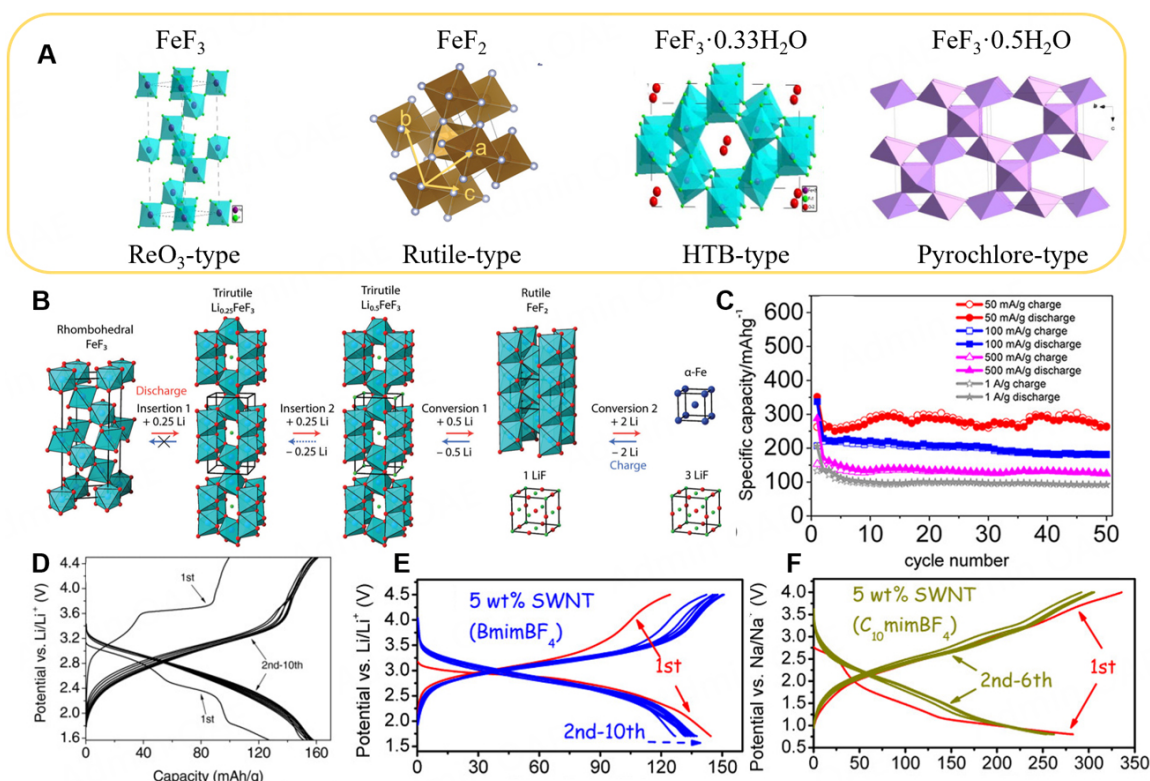
Figure 3. (A) Crystal structures of FeF_3, FeF_2, $FeF_3 \cdot 0.33H_2O$, and $FeF_3 \cdot 0.5H_2O$. This figure is quoted with permission from Liu *et al.* (ReO_3-type and HTB-type)[19], Huang *et al.* (Rutile-type)[25], and Rao *et al.* (Pyrochlore-type)[34]. (B) Reaction pathways for both discharging and charging of the FeF_3 electrode and their crystal structures. These summaries are based on the empirical data and DFT calculation results, where Li, Fe, and F atoms are represented by green, blue, and red spheres. This figure is quoted with permission from Li *et al.*[21]. (C) Performance during cycling of FeF_2@CNT under different current densities, which shows cycling stability and rate performance of FeF_2@CNT. This figure is quoted with permission from Zhou *et al.*[27]. (D) Voltage *vs.* capacity profiles of $FeF_3 \cdot 0.33H_2O$ electrodes for the first ten cycles with a current density of 14 mA g^{-1}. This figure is quoted with permission from Li *et al.*[32]. (E and F) Voltage *vs.* capacity profiles of $FeF_3 \cdot 0.5H_2O$ cathodes wired by 5 wt % SWNTs at 0.1 C during the first few cycles (*vs.* Li/Na Anode, respectively). This figure is quoted with permission from Li *et al.*[29].

gradually reduced to Fe^{2+} as Li^+ is inserted, which is accompanied by the migration of Fe to form FeF_2. The reaction mechanism is closely related to the size of FeF_3 in this process: the FeF_3 at the micrometer scale undergoes a process that involves a two-phase reaction, whereas FeF_3 at the nanoscale displays a mechanism based on a solid solution, suggesting the irreversibility of FeF_3 during charging and discharging may be mitigated by rationally designing FeF_3 nanostructures and reducing the Fe migration distance. FeF_3 nanoparticles (40-106 nm) were prepared in carbon nanocages (40-110 nm) by Yang *et al.* The results showed that the FeF_3 nanoparticles provided an excellent reversible capacity of 410 mAh g^{-1} over 120 cycles at 100 mA g^{-1}[23].

FeF_2 has received attention as an intermediate product of the charge/discharge process of FeF_3. In rutile-type FeF_2, the three-dimensional (3D) network of FeF_6 octahedra is described from trans-chains of edge-sharing octahedra along [001]. The chains are further linked together by opposite vertices (Figure 3A, the second one)[24,25]. FeF_2 also has an excellent theoretical specific capacity (571 mAh g^{-1}), but it shows very poor cycling performance, with a severe decrease in capacity after only five cycles[26]. Its poor cycling performance can be attributed to two main factors. Firstly, the severe volume change that FeF_2 undergoes during the conversion reaction can cause instability. Secondly, FeF_2 dissolves easily in the electrolyte, making it flake off from the current collector. This detachment can disrupt the operation and overall performance. It has

been shown that the cycling performance of FeF_2 in microporous/mesoporous carbon improves dramatically. Zhou *et al.* encapsulated FeF_2 in carbon nanotubes (CNTs)[27]. The CNTs endure the stress brought on by the volume alteration during Li insertion to preserve the shape of the material and secure the contact between the material, the current collector, and the conductive carbon, which enhances the electrochemical performance of FeF_2 [Figure 3C]. In order to reduce the dissolution of FeF_2, Xiao *et al.* used lithium bis(fluorosulfonyl)imide (LiFSI)-based electrolytes to form a protective layer in situ to mitigate the dissolution of the cathode, which successfully enabled the Li-FeF_2 battery to exhibit more than 1,000 stable cycles[28]. Quantum chemical calculations show that the decomposition of LiFSI at the cathode side produces a LiF-rich protective layer.

Another strategy to extend the application of FeF_3 is incorporating structural water. The crystal structure of FeF_3 changes significantly when it contains crystalline water, and several special structures can even accommodate the insertion of Na^+[29]. Hexagonal bronze tungsten (HTB) type $FeF_3 \cdot 0.33H_2O$, which has FeF_6 octahedra connected by shared F atoms to form a hexagonal cavity, forms a tunnel structure along the [001] direction (Figure 3A, the third one)[19,30]. In the tunnel, water molecules occupy 1/3 of the cavity position, and the remaining space can accommodate ion insertion and extraction. This unique structure facilitates rapid ion transport in HTB-type FeF_3[19,30]. Conte *et al.* monitored the reaction by Mossbauer spectroscopy to unveil the reaction mechanism[31]. Their findings implied that during the first discharge, the reduction of Fe^{3+} to Fe^{2+} occurs through two different routes: one portion maintains the original HTB structure, while another portion has a disordered rutile structure. The rutile phase is then restored to the HTB phase during charging. When the voltage is below 2 V, the Fe phase appears, which increases the capacity but decreases the cycling stability. DFT calculations also show that water molecules in $FeF_3 \cdot 0.33H_2O$ are necessary for structural stability, and only $0.66Li^+$ can be inserted to form $Li_{0.66}FeF_3 \cdot 0.33H_2O$[30]. In 2010, Li *et al.* reported a non-aqueous low-temperature synthesis of HTB-FeF_3 based on ionic liquids, which exhibited a capacity of 154 mAh g^{-1} in the first ten cycles, with a typical charge/discharge plateau observed at around 2.7 V without significant polarization during the cycle [Figure 3D][32]. Zhang *et al.* packaged $FeF_3 \cdot 0.33H_2O$ in 3D ordered mesoporous carbon (3D-OMCs) as the cathode material for SIBs, and the first discharge capacity was 386 mAh g^{-1} at a current density of 20 mA g^{-1}, and the capacity was still maintained at 201 mAh g^{-1} at a current density of 100 mA g^{-1}[33]. Such excellent performance was partly attributed to the 3D mesoporous structure of 3D-OMCs, which provides a fast electron diffusion path for Na^+ insertion and extraction. Additionally, the presence of 3D-OMCs alleviates the drastic volume change of $FeF_3 \cdot 0.33H_2O$ during charging and discharging.

The one-dimensional channels of HTB-type $FeF_3 \cdot 0.33H_2O$ indeed facilitate ion transport. However, the single ion channels are easily partially blocked by water molecules, which limits the application of HTB-type FeF_3 in SIBs. When the water of crystallization in FeF_3 increases to 0.5, we get pyrochlore-type $FeF_3 \cdot 0.5H_2O$, whose structure becomes similar to that of $AlF_3 \cdot 0.5H_2O$. FeF_6, as the basic unit in the crystal, is connected to form hexagonal cavities by shared F atoms, and these cavities are connected to form a 3D porous structure (Figure 3A, the last one)[29,34]. This structure has a larger cell volume ($\sim$1,130 $Å^3$) than HTB-FeF_3 (710 $Å^3$) and ReO_3-type FeF_3 (310 $Å^3$). At the same time, the interconnected 3D channels exhibit a higher pore density, which eliminates the need for stringent considerations in terms of pore size, especially for ions with a large radius, such as Na^+[29]. The water molecules in them are limited by the zigzag channels to have less effect on the ion storage. Li *et al.* obtained 10 nm FeF_3 nanospheres with graphene coating in the presence of single-walled CNTs (SWNT), $Fe(NO_3)_3 \cdot 9H_2O$, and the ionic liquid, $BmimBF_4$ or $C_{10}mimBF_4$[29]. The material exhibited excellent lithium storage performance (143 mAh g^{-1} at the first discharge, and the capacity was maintained at 135 mA g^{-1} for the next 300 cycles. Figure 3E) and sodium storage performance (250 mAh g^{-1} at the first discharge, and the capacity was maintained at 150 mAh g^{-1} after 50 cycles. Figure 3F). The

charging and discharging curves show a high degree of symmetry. Beneficial from the open 3D channel, pyrochlore-type $FeF_3 \cdot 0.5H_2O$ exhibits a much smaller polarization than ReO_3-type FeF_3. Jiang *et al.* proposed a pyrochlore-type cathode material, $Fe_2F_5 \cdot H_2O$, for SIBs. This material, benefiting from its large cell volume and interconnected, open 3D channels, facilitates rapid and reversible insertion/extraction of Na^+[35]. The first discharge capacity reached 189.4 mAh g^{-1} at a current density of 20 mA g^{-1}, and it retained a capacity of 147.3 mAh g^{-1} after 30 cycles.

In addition to Fe-based fluorides, Ti, Mn, and Co fluorides were tested for LIBs and SIBs, but none of them can be recharged after the initial discharge[13]. The electrochemical properties of metal fluoride cathodes are summarized in Table 1. Iron-based fluorides show very high specific capacity during charging and discharging, but the occurrence of the conversion reaction will seriously affect the reversibility of the material, and limiting the discharge cutoff voltage to above 2 V can improve the cycling performance but will reduce the energy density, which requires us to make reasonable trade-offs in practical applications. As it does not contain lithium/sodium ions, it needs to be pre-treated when combined with graphite and hard carbon to form a full battery.

Fluorinated polyanionic cathodes
Metal fluorides have great capacity but are limited by their extremely low conductivity and slow kinetics, bringing difficulties in practical applications. In order to take advantage of the high redox potential brought by the high electronegativity of fluorine while waiving the slow kinetics of conversion reactions, researchers have turned their attention to fluorine-based polyanionic compounds. Polyanionic materials exhibit good thermal stability[36,37]. In polyanionic cathode materials, a number of anionic groups are reported ($(XO_4)_m^{n-}$, X = P, S, Si, As, *etc.*)[38,39]. The elevation of the electronegativity of the X atom in the anionic group enhances the ionic character of the redox metal species, thereby increasing the redox potential, which allows us to modulate the working voltage of a material by changing the anionic group type or by combining multiple anionic groups[40]. lithium-/sodium- fluorophosphates ($A_xM_y(PO_4)_mF_n$) and fluorosulfates ($A_xM_y(SO_4)_mF_n$) are the most typical fluorine-based polyanionic compounds in LIBs and SIBs, known for their high operating voltage and excellent thermal stability.

Lithium-/sodium- fluorophosphates ($A_xM_y(PO_4)_mF_n$)
Exploring fluorophosphate chemistry, $LiVPO_4F$ (LVPF) was first introduced as a cathode material for LIBs by Barker *et al.* in 2003[4]. As shown in Figure 4A, $LiVPO_4F$ has a triclinic structure consisting of VO_4F_2 octahedral chains that are interconnected by PO_4 groups to form a 3D framework, of which 18% of the Li occupies the penta-coordination sites (LiO_5) while the remaining 82% occupies the octahedral sites (LiO_6)[41]. During the two-electron transfer (V^{4+} to V^{2+}), there is a 15.9% volume change, exhibiting two distinct redox plateaus observed at 4.2 V and 1.8 V (*vs.* Li^+/Li, Figure 4B)[42].

As analogs to $LiVPO_4F$, $LiFePO_4F$ and $LiTiPO_4F$ share isostructural structures to $LiVPO_4F$[43]. $LiFePO_4F$ can exhibit an insert (extract) Li^+ potential of 2.71 V (*vs.* Li^+/Li) with a first discharge capacity of 129 mAh g^{-1} at a current density of 150 mA g^{-1}[44]. $LiTiPO_4F$ demonstrates two reversible charge/discharge plateaus at 2.8 V and 1.7 V (*vs.* Li^+/Li) and can provide a capacity of 157 mAh g^{-1}[45]. However, their practical application is hindered by the limited energy density caused by a low operating voltage. As fully discharged states (Li-rich states), another type of material known as Li_2MPO_4F (where M can be Mn, Fe, Co, or Ni) holds the potential to reach high energy density by accommodating more than one Li^+ ion on a single transition metal[46,47]. In particular, Li_2CoPO_4F exhibits a high discharge plateau above 4.5 V and good performance (109 mAh g^{-1}) at 2.0-5.5 V (*vs.* Li^+/Li, Figure 4C)[48].

Table 1. Electrochemical properties of typical metal fluorides in lithium-ion batteries.

Materials	Structure	Potential (V *vs.* Li$^+$/Li)	Theoretical capacity (mAh g^{-1})	Theoretical energy density (Wh kg^{-1})	Discharge capacity (mAh g^{-1})
CuF$_2$[17]	Rutile-type	3.55	532	1,874	332
FeF$_3$[13]	ReO$_3$-type	2.74	712	1,950	660
FeF$_2$[27]	Rutile-type	2.66	571	1,518	352
FeF$_3$·0.33H$_2$O[32]	HTB-type	2.9	141	410	386
FeF$_3$·0.5H$_2$O[35]	Pyrochlore-type	3.0	250	750	143
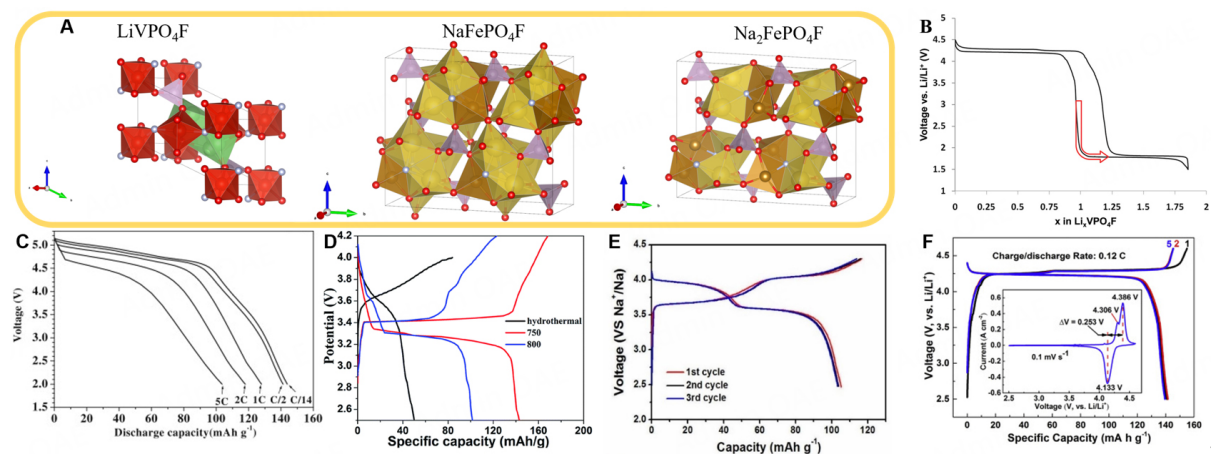
Figure 4. (A) Crystal structures of LiVPO$_4$F, NaFePO$_4$F, and Na$_2$FePO$_4$F. (B) Electrochemical curves of LiVPO$_4$F/C composite cycled *vs.* Li$^+$/Li starting in discharge show Li-ion insertion/extraction potential (as shown by the red arrow). This figure is quoted with permission from Ellis *et al.*[42]. (C) The characteristic discharge profiles of the 5 wt% ZrO$_2$ coated Li$_2$CoPO$_4$F cathode materials between 2 and 5.2 V at various rates. This figure is quoted with permission from Amaresh *et al.*[48]. (D) The charge-discharge curves of NaVPO$_4$F obtained from different synthesis processes at 15 mA g^{-1}. This figure is quoted with permission from Xu *et al.*[49]. (E) Charge-discharge curves of Na$_3$V$_2$PO$_4$F$_3$/C. This figure is quoted with permission from Zou *et al.*[52]. (F) The initial charge/discharge profile of Li$_{0.995}$K$_{0.005}$VPO$_4$F at 0.12 C (1 C = 156 mA g^{-1}) in the potential range of 2.5-4.6 V (*vs.* Li$^+$/Li). The inset shows the CV curves at a scanning rate of 0.1 mV s^{-1}. This figure is quoted with permission from Wu *et al.*[58].

Lithium-/sodium- fluorophosphates are also widely used in SIBs. Similar to LiVPO$_4$F, NaVPO$_4$F is used as a cathode material in SIBs. NaVPO$_4$F has a monoclinic structure with two PO$_4$ tetrahedra, sharing two O atoms connected to two different VO$_4$F$_2$ octahedra[49]. When used as the cathode for SIBs, NaVPO$_4$F synthesized by hydrothermal method showed the best performance, delivering a capacity of ~140 mAh g^{-1} (at 0.1 C) and a discharge plateau of 3.4 V [Figure 4D][49]. In its fully discharged state, Na$_2$FePO$_4$F belongs to the orthorhombic crystal system, which has a layered structure with two different Na sites consisting of FeO$_4$F$_2$ and Fe$_2$O$_7$F$_2$ octahedra[43,50]. This material can exhibit efficient Na$^+$ insertion and extraction at 3.0 V, with an initial discharge capacity of 120 mAh g^{-1}. Besides, Na$_2$MPO$_4$F (M = Co, Mn) with the isostructural structure was also developed[51]. Zou *et al.* synthesized pure Na$_2$CoPO$_4$F by spray drying methods, which exhibit a voltage plateau up to 4.3 V and a discharge capacity of 107 mAh g^{-1}[52]. Wu *et al.* synthesized carbon-coated hollow spheres Na$_2$MnPO$_4$F using the same method, which could observe a plateau of 3.6 V at room temperature and an initial discharge capacity of 102.4 mAh g^{-1} at a current density of 15 mA g^{-1}[53]. As another sodium fluorophosphate with different stoichiometry, Na$_3$V$_2$(PO$_4$)$_2$F$_3$ is a 3D network consisting of [V$_2$O$_8$F$_3$] octahedra and [PO$_4$] tetrahedra. Upon the extraction of two Na$^+$ ions from the framework of Na$_3$V$_2$(PO$_4$)$_2$F$_3$, the material demonstrates dual voltage plateaus at values of 3.7 V and 4.2 V, indicating a theoretical energy density of up to 507 Wh kg^{-1} [Figure 4E][54]. Successful extraction of three Na$^+$ can be achieved when the voltage is extended to 5 V, but this process causes partial structural degradation[55].

The inherently low conductivity discussed above greatly limits the practical application of fluorophosphate materials. In order to solve this obstacle and improve the electrochemical performance, three major strategies with respect to nanostructure engineering, surface coating, and metal doping are developed. Law *et al.* synthesized nano-sized $NaVPO_4F$ with particle sizes ranging from 300-800 nm by the soft template method[56]. Galvanostatic intermittent titration techniques (GITT) revealed that the range of the solid-phase diffusion coefficient D_{Na} was between 2.0×10^{-10}-2.5×10^{-13} cm² s⁻¹. This diffusion coefficient allows the material to be cycled 10,000 times at 10 C and 20 C with capacity retention up to 81% and 87% (1 C = 142 mA g⁻¹). To increase the cycling stability, surface coating is a feasible way to limit the reaction between the cathode material surface and electrolyte. Amaresh *et al.* coated ZrO_2 on the surface of high-voltage Li_2CoPO_4F, and this coating reduced the decomposition of the electrolyte, resulting in an initial discharge capacity of up to 144 mAh g⁻¹ (10 mA g⁻¹)[48]. Metal doping is also an effective method to improve cycling performance, and this method can alter the electronic structure within the material[57]. Various metal substitutions, such as Mg, Cr, Al, and Co, have been unveiled to improve the cycling stability of fluorophosphates. Wu *et al.* compared bare $LiVPO_4F$ with K-doped $Li_{0.995}K_{0.005}VPO_4F$ and found that the K-doped sample exhibited a higher discharge plateau, lower polarization, and lower interfacial impedance[58]. Specifically, it obtained a capacity of 130-140 mAh g⁻¹ at 15 mA g⁻¹ and an average potential of 3.6 V (*vs.* Li⁺/Li, Figure 4F). The almost overlapping charge/discharge curves of the first few cycles demonstrate the high reversibility of the material.

Lithium-/sodium- fluorosulfates ($A_xM_y(SO_4)_mF_n$)
Another promising catalog of the family of fluorosubstituted polyanionic compounds, fluorosulfates, is considered as higher voltage cathode materials for batteries due to the enhanced inductive effect of sulfate than phosphate. Tavorite-type $LiFeSO_4F$, reported as a cathode material for LIBs, has a triclinic crystal structure consisting of shared-angle FeO_4F_2 octahedral chains oriented alternately along the c-axis. These chains connect isolated SO_4 tetrahedra to form a 3D framework and form diffusion channels along the [110], [010], and [101] directions [Figure 5A][59-61]. In LIBs, it exhibits a reversible capacity of 130-140 mAh g⁻¹ (at 15 mA g⁻¹) and an average potential of 3.6 V [Figure 5B]. In addition to Tavorite-type $LiFeSO_4F$, triplite-type $LiFeSO_4F$ is also a reported cathode material for LIBs. Unlike tavorite-type $LiFeSO_4F$, triplite-type $LiFePO_4F$ exhibits co-edge connections between FeO_4F_2 octahedra and LiO_4F_2 octahedra. This connection changes the conformation of F atoms around Fe, causing electrostatic repulsion, thereby making triplite-type $LiFeSO_4F$ exhibit higher operating voltage (3.9 V *vs.* Li⁺/Li). A similar structure of triplite-type $NaFeSO_4F$ was also investigated for its sodium storage properties[5]. In contrast, $NaFeSO_4F$ exhibits a smaller tunnel angle of 75 (85) and a larger tunnel size due to the larger radius of Na[5,60]. $NaFeSO_4F$ has a high operating voltage (3.7 V *vs.* Na⁺/Na) but exhibits a coulombic efficiency of about 78% and an energy efficiency of 64% during cycling [Figure 5C], which is mainly due to the severe distortion of the crystal structure occurring upon Na-ion insertion[62]. Notably, unlike the 3D tunnel of $LiFeSO_4F$, it has been demonstrated that $NaFeSO_4F$ conducts Na-ions in a one-dimensional manner through the [101] tunnel. Not only Fe-based fluorosulfates but also fluorosulfate materials based on other transition metals have been examined, such as tavorite $LiCoSO_4F$, triplite $LiMnSO_4F$, and sillimanite $LiZnSO_4F$[63]. Unfortunately, none of them are electrochemically active.

Besides the above-mentioned crystalline fluorosulfides, amorphous fluorosulfates have also received attention from researchers. Heo *et al.* reported a-$LiFeSO_4F$, a stable and reversible amorphous fluorinated iron sulfate electrode[64]. During the discharge process, the amorphous $LiFeSO_4F$ consists of two processes that can be represented by the following equation:

a-FeSO$_4$ + Li$^+$ → LiFeSO$_4$ (Intercalation reaction at ~3.59 V *vs.* Li$^+$/Li)

b-LiFeSO$_4$F + 2Li$^+$ + 2e$^-$ → Fe + LiFeSO$_3$F + Li$_2$O (Conversion reaction at ~2.18 V *vs.* Li$^+$/Li)

This mechanism is also evidenced by the dQ/dV profile [Figure 5D], where sharp redox peaks can be observed at 3.6 V and 3.9 V for tavorite- and triplite-type LiFeSO$_4$F, but a-LiFeSO$_4$F does not display similar peaks in this interval; instead, it exhibits a clear redox peak at 2.2 V and a capacity of 300 mAh g^{-1} at 25 °C (current density: 40 mA g^{-1}) without significant capacity attenuation in 200 cycles [Figure 5E]. The superior cycling stability can be credited to the distinctive amorphous structure of a-LiFeSO$_4$F that can remain intact after the conversion reaction and serve as the main host for subsequent Li$^+$ insertion.

The electrochemical properties of fluorinated polyanionic compounds are summarized in Table 2. It can be seen that these electrodes generally have high operating voltages. Additionally, they also have good cycling performance and thermal stability due to their stable structural framework.

THE ROLE OF FLUORINE IN ELECTROLYTES AND INTERFACE

The electrolyte undertakes the function of ion transport, so the stability of the electrolyte and its properties are crucial to the performance of the battery[7]. The introduction of fluorine into the electrolyte and the construction of a robust EEI are two effective ways from the application perspective. The introduction of fluorine can improve the oxidative stability of the electrolyte. At the same time, the introduction of fluorine into the electrolyte can change the physicochemical properties of the electrolyte, such as melting point, flash point, *etc.*, which makes the electrolyte have some unique functions, such as a wide range of operating temperatures, high safety, *etc*. The construction of a stable EEI can overcome the thermodynamic instability between the electrolyte and the electrode, promote the uniform deposition of ions, and reduce the loss of active metals.

Functionalized fluorinated electrolytes

Functionalized fluorinated electrolytes could extend the application scenarios of rechargeable batteries, such as high/low temperature operation, high safety, high power, *etc.*, as discussed below:

Previous studies have shown that fluorinated solvents can effectively enhance the low-temperature performance of electrolytes. The substitution of fluorine typically lowers the freezing point of most solvents, enhancing the conductivity of the electrolyte during cold temperatures. This, in turn, improves the battery performance under low-temperature conditions. Fluorine, as a strong electron absorbing group, weakens the electron-giving ability of the solvent/co-solvent when there is a fluorine substitution on them. Fluorine-substituted solvent/co-solvent molecules have lower binding energies (in absolute terms) when coordinated with Li$^+$, which means that introducing fluorine into solvent/co-solvent molecules can make it easier to detach Li$^+$ from the solvation structure[65]. Yang *et al.* proposed an ethyl trifluoroacetate (ETFA)-based electrolyte[66]. Due to the high electronegativity of the fluorine, the binding energy of this solvent to Li$^+$ is much lower than that of ethylene carbonate (EC), which allows the rapid de-solvation of Li$^+$ from the solvation structure. Owing to the fast de-solvation process, Li||LTO cells with this electrolyte achieve capacities of 154 mAh g^{-1} and 78 mAh g^{-1} at -50 °C and -70 °C, respectively [Figure 6A].

Introduction of fluorinated molecules into the electrolyte also could extend the high temperature adaptability. Generally, organic molecules become less combustible as the degree of F substitution increases, which makes the electrolyte safer[67]. In addition, F atoms also have a strong attraction to H atoms, which allows F to absorb H radicals during combustion and quench the chain reaction, increasing the flash point

Table 2. Electrochemical performance of fluorinated polyanionic cathodes

Materials	Structure	Potential (V *vs.* Li$^+$/Li or Na$^+$/Na)	Theoretical capacity (mAh g^{-1})	Theoretical energy density (Wh kg^{-1})	Discharge capacity (mAh g^{-1})
LiVPO$_4$F[41]	Tavorite	4.2	237	995	106
LiFePO$_4$F[44]	Tavorite	2.71	151	409	129
LiTiPO$_4$F[45]	Tavorite	2.8/1.7	161	326	149
Li$_2$CoPO$_4$F[48]	Orthorhombic	4.5	143	643	91
LiFeSO$_4$F[61]	Tavorite-type	3.6	150	542	130
a-LiFeSO$_4$F[64]	Amorphous	2.5 V	454	1,135	300
NaVPO$_4$F[49]	Tavorite	3.4	142	482	121
Na$_2$FePO$_4$F[43]	Orthorhombic	3.0	124	372	121
Na$_2$MnPO$_4$F[43]	Orthorhombic	3.6	124	449	99
Na$_3$V$_2$(PO$_4$)$_2$F$_3$[55]	Tetragonal	3.7/4.2	128	507	110
NaFeSO$_4$F[62]	Triplite	3.5 V	138	483	83
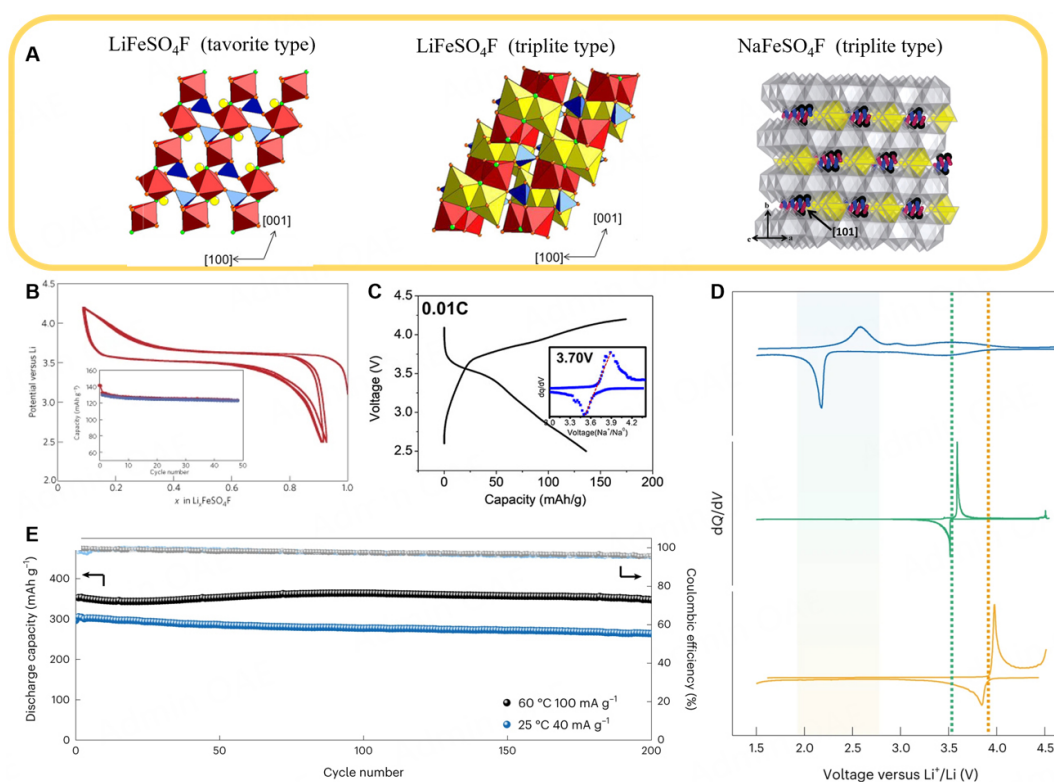
Figure 5. (A) Crystal structures of tavotite and triplite-type LiFeSO$_4$F and triplite-type type NaFeSO$_4$F. This figure is quoted with permission from Ati *et al.*[59]. and Tripathi *et al.*[60]. (B) The tavorite LiFeSO$_4$F has a stable cycling performance. Charge/discharge profile of LiFeSO$_4$F cells cycled between 2.5 and 4.2 V at 15 mA g^{-1}. This figure is quoted with permission from Recham *et al.*[61]. (C) Charge and discharge profiles for triplite-type NaFeSO$_4$F discharge at 0.01 C (1C = 138 mA g^{-1}). This figure is quoted with permission from Kim *et al.*[62]. (D) a-LiFeSO$_4$F shows a different charge/discharge mechanism compared to tavotite and triplite-type LiFeSO$_4$F. dQ/dV profile of a-LiFeSO$_4$F (blue), tavorite (green), and triplite (orange). This figure is quoted with permission from Heo *et al.*[64]. (E) Cycling performance of a-LiFeSO$_4$F at different temperatures measured at a current density of 40 mA g^{-1}. This figure is quoted with permission from Heo *et al.*[64].

and flame retardant properties of the solvent [Figure 6B]. An ultra-concentrated electrolyte composed of LiFSA and fluorinated alkyl phosphate was prepared by Shiga *et al.* This electrolyte was self-extinguishing and allowed reversible insertion of Li$^+$ into graphite, and the electrolyte also exhibited ultra-high thermal
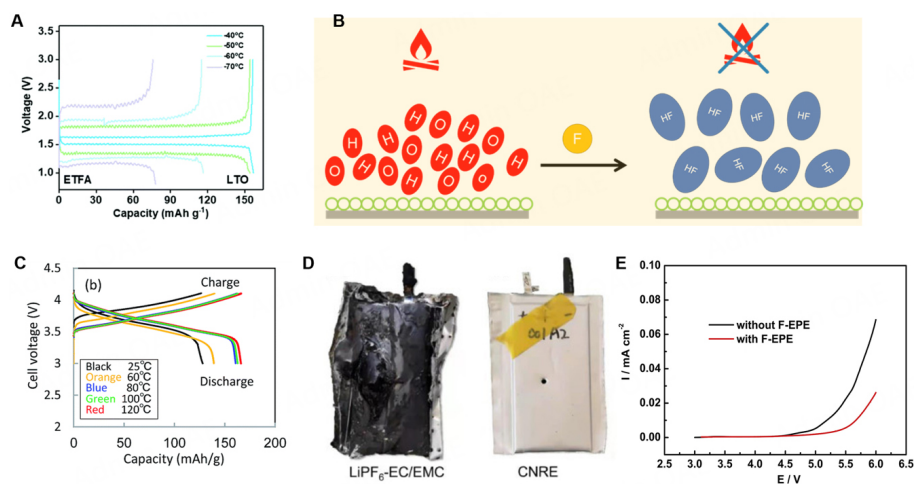
Figure 6. (A) Charge/discharge profiles of LTO||Li cells using the ETFA electrolyte under different temperatures. This figure is quoted with permission from Yang *et al.*[66]. (B) Schematic diagram of fluorine flame retardant principle; (C) Charge/discharge profiles of the LiNi$_{0.8}$Co$_{0.15}$Al$_{0.05}$O$_2$/Li half cells at various temperatures, which demonstrates the excellent high temperature stability of fluorinated solvents. This figure is quoted with permission from Shiga *et al.*[68]. (D) Nail penetration tests of the 5 Ah graphite||NMC pouch use LiPF$_6$-EC/EMC (left) and coordination number-rule electrolyte. This figure is quoted with permission from Chen *et al.*[69]. (E) The linear sweep voltammetry curves of the electrolyte without and with F-EPE, which shows fluoride electrolytes could operate under high potential. This figure is quoted with permission from Luo *et al.*[73].

stability. Such features allow graphite/Li half-cells with this electrolyte to operate at temperatures exceeding 100 °C [Figure 6C][68]. Our group has proposed an electrolyte using trifluoroethyl phosphate and trifluoroethyl methyl carbonate as solvents. After nail penetration, pouch cells using this electrolyte still keep compact, while pouch cells using commercial 1m LiPF$_6$-EC/EMC (EMC: Ethyl Methyl Carbonate) electrolytes immediately catch fire [Figure 6D][69]. Notably, due to the advantages of the F-substitute solvent described earlier, the pouch battery using the electrolyte can also operate stably within a temperature range of -40-60 °C.

The electron-withdrawing inductive effect results in a decrease in the highest occupied molecular orbital (HOMO) and the lowest unoccupied molecular orbital (LUMO) energy levels when fluorine is introduced into the solvent molecule[70,71]. The decrease of the HOMO energy level enhances the anti-oxidative properties of the molecule, which enables this substance to be compatible with high potential cathodes, thus meeting the high-energy requirements[72]. Luo *et al.* expanded the electrochemical window by adding 10% of fluorinated 3-(1,1,2,2-tetrafluoroethoxy)-1,1,2,2-tetrafluoropropane (F-EPE) solvent to 1.2 M LiPF$_6$ in EC/EMC electrolytes[73]. With the introduction of F-EPE, the potential window of the electrolyte extends above 5.2 V [Figure 6E]. This high potential window allows Li||LiNi$_{0.5}$Mn$_{1.5}$O$_4$ cells to have higher stability and coulombic efficiency.

Fluorinated interface engineering
Briefly, the essence of the formation of the EEI is a redox reaction between the electrode and the electrolyte[8]. Taking LIBs as an example, SEI has many components, such as Li$_2$O, LiOH, Li$_2$CO$_3$, Li$_3$N, *etc.*[74,75]. Among them, LiF has attracted a lot of attention due to its excellent performance. As a SEI component, LiF has a wide band gap (8.70 eV) to effectively prevent electron transport[76]. At the same time, the high mechanical strength and low solubility of LiF make the LiF-rich interface extremely stable[77,78]. The safety of the battery can be enhanced through the efficient inhibiting of dendrite growth on the electrode surface by the high surface energy and low diffusion energy of LiF-rich SEI[79].

HOMO and LUMO directly reflect the redox stability of the electrolyte. Meanwhile, both the cathode and anode have their own electrochemical potentials[80]. If the anode potential is higher than LUMO, then the electrons on the anode will tend to transfer to the electrolyte, thus causing the electrolyte to reduce, creating a solid-electrolyte interface and preventing the reaction from proceeding further. A similar situation occurs at the cathode, creating a cathode-electrolyte interface (CEI) [Figure 7A][81]. In addition to preventing the electrolyte from further decomposition, the current study also found that a fluorinated interface has a positive role in protecting the electrodes and promoting the uniform deposition of Li [Figure 7B][82].

Many efforts have been made by researchers to obtain stable fluorinated interfaces. The straight ward method to get robust EEI is pretreatment by ex-situ coating a layer of LiF on Cu or Li to improve electrochemical performance. Zhang *et al.* plated LiF on the surface of Cu collectors[83]. LiF-rich SEIs guided the deposited Li into a stabilized structure, which greatly contributed to the stability of such anodes. Zhao *et al.* developed a method to form LiF films using the fluoropolymer CYTOP as a precursor to generate F_2 *in situ* [Figure 7C][84]. This compound can release F_2 at less than 250 °C, thereby generating a dense LiF coating on the anode. This film is able to minimize the interaction between lithium metal and carbonate electrolyte, preventing the creation of dendrites and leading to 300 cycles without dendrite formation at a current density of 5 mA cm^{-2}.

The second way to generate a fluorinated interface is from organic components (either organic additives or solvents). As we mentioned before, fluorine substitution reduces the LUMO energy levels of the components in the electrolyte, which makes the fluorinated electrolyte components easier to reduce and thus generate stable SEIs[70]. In addition, theoretical calculations also show that fluorinated solvent molecules that are in the primary solvated shell layer of the Li cation are more easily reduced[8]. EC is the most widely used solvent commercially, and its fluorine-substituted product, fluoroethylene carbonate (FEC), is the most widely used film-forming additive for a variety of batteries, including LIBs, LMBs, and SIBs[85-87]. Wen *et al.* prepared hollow carbon nanospheres as anodes for SIBs and achieved a specific capacity of 89.9 mAh g^{-1} at 5 A g^{-1} by introducing 2 vol.% FEC into the electrolyte [Figure 7D][88]. In LMBs, FEC can also form a dense and stable protective film on the lithium metal surface. Zhang *et al.* obtained a homogeneous SEI by introducing a small amount of FEC (5%) into the EC-based electrolyte[86]. This homogeneous SEI significantly improved the Coulombic efficiency of the Li||Cu half-cells (Coulombic efficiency of 98% within 100 cycles, Figure 7E). Matching the FEC-protected lithium metal with $LiNi_{0.5}Co_{0.2}Mn_{0.3}O_2$ resulted in an initial capacity of up to 154 mAh g^{-1}. Silicon is considered a promising anode for the new generation of high-specific-energy LIBs. However, it undergoes significant volume changes when it charges and discharges. Researchers found that adding FEC to the electrolyte could generate smoother, more stable SEI on the Si anode, and subsequent studies have further demonstrated that FEC in the electrolyte can form a fluorinated interface on the Si anode or Si-graphite, thus preventing further side-reactions during the volume change[89,90].

To improve the effectiveness of FEC, the researchers increased the amount of FEC in the electrolyte. Lee *et al.* proposed a series of FEC, DEC-based electrolytes with different FEC contents[85]. By introducing FEC, the reversibility of the Li anode was significantly improved. This electrolyte effectively improved the coulombic efficiency and cycling performance of Li/LiCoO$_2$ (LCO) batteries (30% FEC, capacity retention of 97.5% for 900 cycles, Coulombic efficiency: 99.0%, Figure 7F). However, the amount of FEC is not the more, the better; when the FEC content reaches more than 50%, the battery efficiency and capacity will produce a significant decrease, which is due to the formation of a resistive layer on the surface of LCO by FEC and, thus, significantly reduce the discharge capacity.
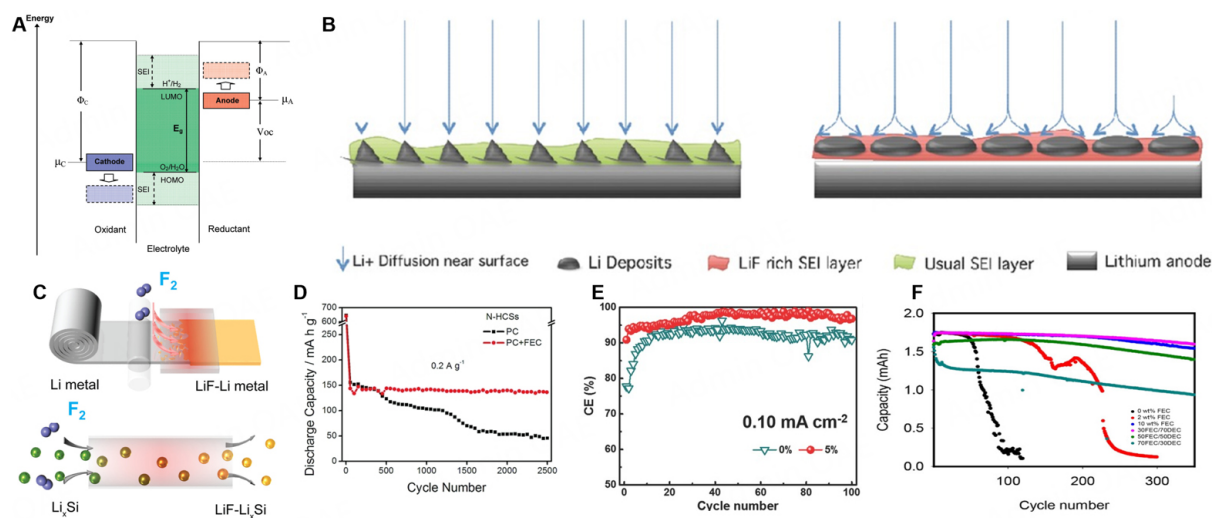
Figure 7. (A) Schematic diagram of the mechanism of SEI and CEI formation. This figure is quoted with permission from Goodenough *et al.*[81]. (B) Schematic of how LiF-rich SEI prevents the growth of dendrites. This figure is quoted with permission from Choudhury *et al.*[82]. (C) The schematic shows that when heated, the fluoropolymer, CYTOP, gradually breaks down to release pure F_2 gas. This gas then reacts with lithium metal or Li_xSi, resulting in a uniform and dense coating of LiF. This figure is quoted with permission from Zhao *et al.*[84]. (D) Long-term cycling stabilities of anode at a current rate of 0.2 A g^{-1} in 1m NaClO$_4$ electrolyte in PC without and with 2 vol.% of FEC additive. This figure is quoted with permission from Wen *et al.*[88].(E) Coulombic efficiency of Li‖Cu battery at a current density of 0.10 mA cm^{-2}. This figure is quoted with permission from Zhang *et al.*[86].(F) Discharge capacities of the Li/LCO cells cycled at 1.0 C (1 C = 274 mA g^{-1}). This figure is quoted with permission from Lee *et al.*[85].

The third strategy for achieving a fluorinated interface comes from the inorganic component. The salt is another important component in the electrolyte. It has been shown that most of the F-containing lithium salts (e.g., LiPF$_6$, LiBF$_4$, LiFSI, *etc.*) can involve the F in them in the generation of LiF-rich SEI[91-93]. The decomposition of these salts produces an electrodeless fluorinated interface with excellent physical and chemical properties. Chen *et al.* designed an electrolyte [2.0 m LiPF$_6$ in 1:1 v/v mixture of tetrahydrofuran and 2-methyltetrahydrofuran (mixTHF)][76]. The use of ether with a low thermodynamic reduction potential (0.0-0.3 V *vs.* Li$^+$/Li) as a solvent allowed PF$_6^-$ to become preferentially decomposed relative to being in a carbonate-based electrolyte [Figure 8A-C]. The SEI produced by the decomposition of inorganic salts greatly improves the cycling stability of the battery.

When the salt concentration is increased, the anion decomposition tendency will be improved. DFT-molecular dynamics (MD) simulations illustrate that the LUMO energy level of the electrolyte gradually shifts from the solvent to the anion when the salt concentration is gradually increased [Figure 8D and E][94]. Wang *et al.* developed highly concentrated electrolytes for LIBS and SIBs, using trimethyl phosphate (TMP) as solvents and NaN(SO$_2$F)$_2$ (NaFSA) or LiN(SO$_2$F)$_2$ (LiFSA) as salts[95]. Both electrolytes showed excellent performance (almost no degradation for 1,000 cycles, Figure 8F) when the NaFSA and LiFSA concentrations were increased to 3.3 m and 5.3 m, respectively.

The excellent SEI brought by high concentration electrolytes can significantly improve battery performance, but the higher viscosity and cost greatly limit the practical application of high concentration electrolytes. To address these two drawbacks, researchers have proposed an electrolyte known as localized high concentration electrolyte (LHCE). By adding one or more diluents that are immiscible with salt but miscible with solvents to the electrolyte, the electrolyte is saturated at a low concentration and exhibits low viscosity and ionic conductivity. Piao *et al.* added 1,1,2,2-Tetrafluoroethyl-2,2,3,3-tetrafluoropropylether (TTE) as a diluent to LiFSI/DMC electrolyte to form LHCE[96]. MD simulations revealed that the introduction of
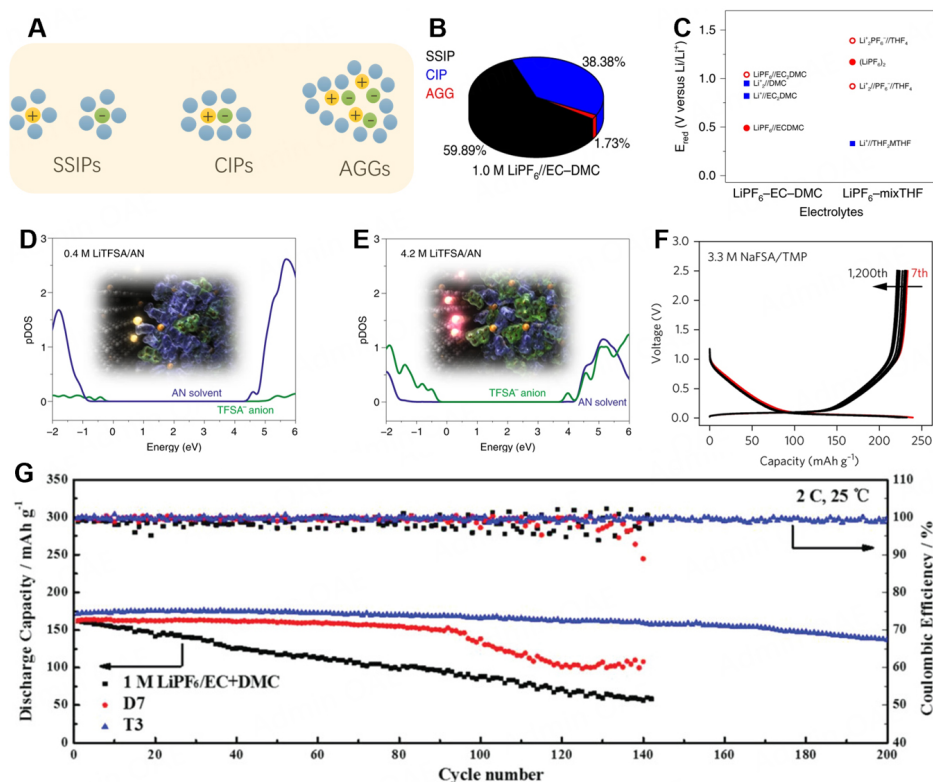
Figure 8. (A) Schematic of three general categories of solvent-salt interactions. (B) Distribution of the Li^+ solvates for the $LiPF_6$-THF (2.0 M) from MD simulations. This figure is quoted with permission from Chen *et al.*[76]. (C) Reduction potentials of key electrolyte components with the first Li^+ solvation shell, which shows that fluorinated salts will decompose preferentially. This figure is quoted with permission from Chen *et al.*[76]. (D and E) Calculated electronic structures (projected density of states, pDOS) of dilute D and concentrated E LiTFSA/AN electrolytes, which suggests a gradual transfer of LUMO to anion with increasing concentration. This figure is quoted with permission from Yamada *et al.*[94]. (F) Charge/discharge profiles of Na||HC(hard carbon) cells using the concentrated NaFSA/TMP electrolyte. This figure is quoted with permission from Wang *et al.*[95]. (G) Cycling performance with different electrolytes at 2 C and 25 °C. This figure is quoted with permission from Piao *et al.*[96].

diluent enhances the interaction between Li^+ and FSI^- so that the FSI^- can be preferentially reduced to form LiF-rich SEI. This electrolyte enables stable cycling of Li||NMC622 cells at both 25 and 60 °C [Figure 8G].

CONCLUSION AND OUTLOOK

Fluorine chemistry plays a pivotal role in the pursuit of high energy density, high stability, and high safety batteries. Figure 9 displays a comprehensive comparison of the potential, specific capacity, and specific energy images of fluorinated electrodes. Transition metal fluorides exhibit excellent specific capacity and specific energy through conversion reactions, and fluorinated polyanion compounds have higher operating voltages as a consequence of the inductive effect of F^-. Fluorinated polyanionic compounds also have a high working potential due to the inductive effect of fluorine, while the stable backbone can withstand the insertion/extraction of lithium-/sodium- ions in them. However, the introduction of fluorine also poses challenges for both types of materials. The high electronegativity of fluorine gives transition metal fluorides and fluorinated polyanion compounds very low conductivity, which results in very high polarization during charging and discharging. Transition metal fluorides also suffer from uneven distribution of the active substance, severe volume changes, and dissolution of the active substance in the conversion reaction.
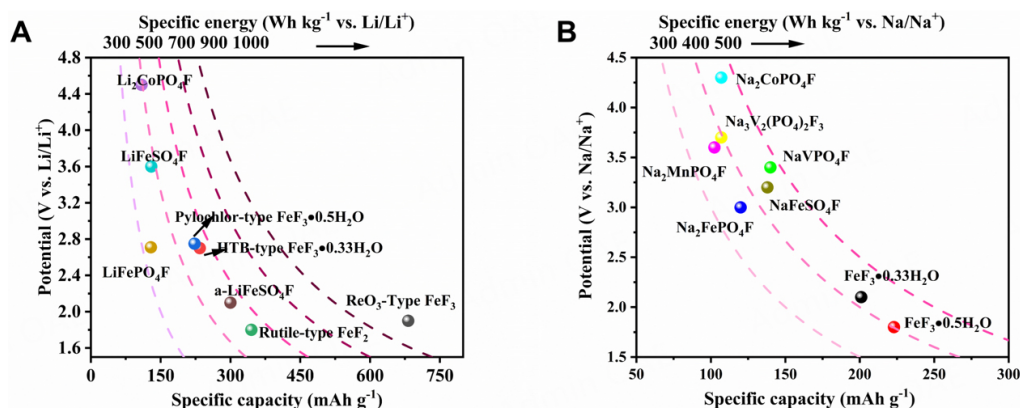
Figure 9. Comparisons among fluorinated electrode materials for (A) LIBs, (B) SIBs.

Aiming to facilitate fluorinated electrodes towards practical applications, more efforts should be devoted to the following topics:

(1) Transition metal fluorides generally cannot supply lithium ions; hence, they are unable to couple with lithium-free anodes, such as graphite and silicon, in LIBs. Nevertheless, if matched with lithium metal anode in solid-state lithium batteries, the high-capacity advantage of the fluoride cathodes will be more prominent. One thing that needs to be emphasized is that the sluggish reaction kinetics and large voltage hysteresis of transition metal fluoride cathodes always lead to low energy conversion efficiency and insufficient output power, which is detrimental to their competitiveness.

(2) Fluorinated polyanionic cathode materials have received particular attention in SIBs due to their superiority of high operating voltage compared to the commonly studied layered transition metal oxides and Prussian blue analog cathodes. To pursue high electrochemical performance, strategies such as structural regulation and morphology tailoring are often incorporated into the synthesis procedure of fluorinated materials, which would undoubtedly bring increased manufacturing costs.

(3) Only in at least Ah-grade batteries can we accurately evaluate the practical electrochemical properties of fluorinated electrodes; the data obtained from the button battery test are not representative and may even be deceptive. In addition, fluoride ions involved in cathode materials may cause safety and environmental issues in material production, battery manufacturing, and recycling processes, which should be paid more attention to.

Fluorine also occupies a pivotal position in functional electrolytes. The physical and chemical properties of electrolyte solvents are significantly altered after fluorine-containing components are incorporated. The lower freezing point and the ability to bond with cations enable the fluorine electrolyte to exhibit excellent performance at low temperatures. The flame retardant property of fluorine also makes the electrolyte show excellent safety performance at high temperatures. The decreased HOMO energy level allows the electrolyte to operate at higher voltages, thus realizing high specific energy.

Regarding the EEI, a fluorinated interface is essential due to its high ionic conductivity, electron insulation, and mechanical robustness. A stable EEI could be built from the electrolyte by designing solvated structures.

Although fluorinated electrolytes have made remarkable contributions to the advances in battery technology, their potential has not yet been fully explored. Future research should focus on the following aspects.

(1) Fluorine-containing components in the electrolyte, such as salts, solvents, additives, *etc.*, enable LIBs and SIBs to achieve improved performance, but their potential toxicity and corrosion will also raise concerns; hence, robust battery pack components should be rationally designed, and advanced battery recycling technologies should be developed.

(2) The interaction between solvents and salts greatly affects the performance of electrolytes. Considering the complexity and variability of the electrolyte composition, it is not a realistic way to optimize the composition of the electrolyte through experiments. Theoretical calculations, such as MD simulations and DFT, are powerful tools to investigate the intermolecular interactions in electrolytes. The in-depth inspection of the solvation structure can provide theoretical guidance for us to better design functionalized electrolytes.

(3) Fluorinated components endow the electrode/electrolyte interfaces with excellent mechanical/chemical/ electrochemical stability. However, the interface is susceptible to electron radiation, X-rays, oxygen, and moisture and gradually ages during the cycle, causing a decline in battery performance. Therefore, monitoring the evolution of interface composition and structure is the basis for designing a robust and reliable interface.

In this review, we discuss the characteristics of fluorine and its unique role in the electrode, electrolyte, and EEI. The high electronegativity and strong inductive effect of fluorine can effectively increase the electrode operating voltage, and the strong electron-absorbing tendency of fluorine in the electrolyte can give the electrolyte the advantages of wide operating temperature and high potential window. The characteristics of LiF, such as wide forbidden band, high ion diffusion rate, low solubility, and high Young's modulus, make LiF a star component of EEIs. These unique roles of fluorine presented here may provide new ideas for future battery design.

DECLARATIONS

Authors' contributions
Proposed the topic of this review: Chen Z
Prepared the manuscript: Pan Z, Pu X
Collectively discussed and revised the manuscript: Pan Z, Chen H, Zeng Y, Ding Y, Pu X, Chen Z

Availability of data and materials
Not applicable.

Conflicts of interest
All authors declared that there are no conflicts of interest.

Ethical approval and consent to participate

Not applicable.

Consent for publication

Not applicable.

Copyright

© The Author(s) 2023.

REFERENCES

1.   Ullah N, Guziejewski D, Yuan A, Shah SA. Recent advancement and structural engineering in transition metal dichalcogenides for alkali metal ions batteries. *Materials* 2023;16:2559. DOI PubMed PMC

2.   Li H, Richter G, Maier J. Reversible formation and decomposition of LiF clusters using transition metal fluorides as precursors and their application in rechargeable Li batteries. *Adv Mater* 2003;15:736-9. DOI

3.   Arai H, Okada S, Sakurai Y, Yamaki J. Cathode performance and voltage estimation of metal trihalides. *J Power Sources* 1997;68:716-9. DOI

4.   Barker J, Saidi MY, Swoyer JL. Electrochemical insertion properties of the novel lithium vanadium fluorophosphate, $LiVPO_4F$. *J Electrochem Soc* 2003;150:A1394. DOI

5.   Tripathi R, Ramesh TN, Ellis BL, Nazar LF. Scalable synthesis of tavorite $LiFeSO_4F$ and $NaFeSO_4F$ cathode materials. *Angew Chem Int Ed* 2010;49:8738-42. DOI PubMed

6.   Xu ZL, Yoon G, Park KY, et al. Tailoring sodium intercalation in graphite for high energy and power sodium ion batteries. *Nat Commun* 2019;10:2598. DOI PubMed PMC

7.   von Aspern N, Röschenthaler GV, Winter M, Cekic-Laskovic I. Fluorine and lithium: ideal partners for high-performance rechargeable battery electrolytes. *Angew Chem Int Ed* 2019;58:15978-6000. DOI PubMed

8.   Tan J, Matz J, Dong P, Shen J, Ye M. A growing appreciation for the role of LiF in the solid electrolyte interphase. *Adv Energy Mater* 2021;11:2100046. DOI

9.   Sun L, Li Y, Feng W. Metal fluoride cathode materials for lithium rechargeable batteries: focus on iron fluorides. *Small Methods* 2023;7:e2201152. DOI

10. Lemoine K, Hémon-Ribaud A, Leblanc M, Lhoste J, Tarascon JM, Maisonneuve V. Fluorinated materials as positive electrodes for Li- and Na-ion batteries. *Chem Rev* 2022;122:14405-39. DOI

11. Li T, Chen ZX, Ai XP, Cao YL, Yang HX. LiF/Fe nanocomposite as a lithium-rich and high capacity conversion cathode material for Li-ion batteries. *J Power Sources* 2012;217:54-8. DOI

12. Badway F, Cosandey F, Pereira N, Amatucci GG. Carbon metal fluoride nanocomposites: high-capacity reversible metal fluoride conversion materials as rechargeable positive electrodes for Li batteries. *J Electrochem Soc* 2003;150:A1318. DOI

13. Liu S, Chen Z, Xie K, Li Y, Xu J, Zheng C. A facile one-step hydrothermal synthesis of α-Fe_2O_3 nanoplates imbedded in graphene networks with high-rate lithium storage and long cycle life. *J Mater Chem A* 2014;2:13942-8. DOI

14. Wang F, Robert R, Chernova NA, et al. Conversion reaction mechanisms in lithium ion batteries: study of the binary metal fluoride electrodes. *J Am Chem Soc* 2011;133:18828-36. DOI

15. Yamakawa N, Jiang M, Grey CP. Investigation of the conversion reaction mechanisms for binary copper(II) compounds by solid-state NMR spectroscopy and X-ray diffraction. *Chem Mater* 2009;21:3162-76. DOI

16. Hua X, Robert R, Du L, et al. Comprehensive study of the CuF_2 conversion reaction mechanism in a lithium ion battery. *J Phys Chem C* 2014;118:15169-84. DOI

17. Seo JK, Cho HM, Takahara K, et al. Revisiting the conversion reaction voltage and the reversibility of the CuF_2 electrode in Li-ion batteries. *Nano Res* 2017;10:4232-44. DOI

18. Wang F, Kim SW, Seo DH, et al. Ternary metal fluorides as high-energy cathodes with low cycling hysteresis. *Nat Commun* 2015;6:6668. DOI PubMed PMC

19. Liu L, Guo H, Zhou M, et al. A comparison among FeF_3·$3H_2O$, FeF_3·$0.33H_2O$ and FeF_3 cathode materials for lithium ion batteries: structural, electrochemical, and mechanism studies. *J Power Sources* 2013;238:501-515. DOI

20. Amatucci GG, Pereira N. Fluoride based electrode materials for advanced energy storage devices. *J Fluor Chem* 2007;128:243-62. DOI

21. Li L, Jacobs R, Gao P, et al. Origins of large voltage hysteresis in high-energy-density metal fluoride lithium-ion battery conversion electrodes. *J Am Chem Soc* 2016;138:2838-48. DOI

22. Hua X, Eggeman AS, Castillo-Martínez E, et al. Revisiting metal fluorides as lithium-ion battery cathodes. *Nat Mater* 2021;20:841-50. DOI

23. Yang Y, Gao L, Shen L, Bao N. Self-assembled FeF_3 nanocrystals clusters confined in carbon nanocages for high-performance Li-ion battery cathode. *J Alloy Compd* 2021;873:159799. DOI

24. Santos-Ortiz R, Volkov V, Schmid S, et al. Microstructure and electronic band structure of pulsed laser deposited iron fluoride thin

film for battery electrodes. *ACS Appl Mater Interfaces* 2013;5:2387-91. DOI

25. Huang Q, Pollard TP, Ren X, et al. Fading mechanisms and voltage hysteresis in FeF_2-NiF_2 solid solution cathodes for lithium and lithium-ion batteries. *Small* 2019;15:e1804670. DOI

26. Li H, Balaya P, Maier J. Li-storage via heterogeneous reaction in selected binary metal fluorides and oxides. *J Electrochem Soc* 2004;151:A1878. DOI

27. Zhou J, Zhang D, Zhang X, Song H, Chen X. Carbon-nanotube-encapsulated FeF_2 nanorods for high-performance lithium-ion cathode materials. *ACS Appl Mater Interfaces* 2014;6:21223-9. DOI

28. Xiao AW, Lee HJ, Capone I, et al. Understanding the conversion mechanism and performance of monodisperse FeF_2 nanocrystal cathodes. *Nat Mater* 2020;19:644-54. DOI

29. Li C, Yin C, Gu L, et al. An $FeF_3 \cdot 0.5H_2O$ polytype: a microporous framework compound with intersecting tunnels for Li and Na batteries. *J Am Chem Soc* 2013;135:11425-8. DOI

30. Li Z, Wang B, Li C, Liu J, Zhang W. Hydrogen-bonding-mediated structural stability and electrochemical performance of iron fluoride cathode materials. *J Mater Chem A* 2015;3:16222-8. DOI

31. Conte DE, Di Carlo L, Sougrati MT, Fraisse B, Stievano L, Pinna N. Operando mössbauer spectroscopy investigation of the electrochemical reaction with lithium in bronze-type $FeF_3 \cdot 0.33H_2O$. *J Phys Chem C* 2016;120:23933-43. DOI

32. Li C, Gu L, Tsukimoto S, van Aken PA, Maier J. Low-temperature ionic-liquid-based synthesis of nanostructured iron-based fluoride cathodes for lithium batteries. *Adv Mater* 2010;22:3650-4. DOI PubMed

33. Zhang R, Wang X, Wang X, et al. Iron fluoride packaged into 3D order mesoporous carbons as high-performance sodium-ion battery cathode material. *J Electrochem Soc* 2018;165:A89. DOI

34. Rao R, Pralong V, Varadaraju U. Facile synthesis and lithium reversible insertion on iron hydrated trifluorides $FeF_3 \cdot 0.5H_2O$. *Mater Lett* 2016;170:130-4. DOI

35. Jiang M, Wang X, Shen Y, Hu H, Fu Y, Yang X. New iron-based fluoride cathode material synthesized by non-aqueous ionic liquid for rechargeable sodium ion batteries. *Electrochim Acta* 2015;186:7-15. DOI

36. Liu Y, Li J, Shen Q, et al. Advanced characterizations and measurements for sodium-ion batteries with NASICON-type cathode materials. *eScience* 2022;2:10-31. DOI

37. Wang H, Pan Z, Zhang H, et al. A green and scalable synthesis of $Na_3Fe_2(PO_4)_2P_2O_7$/rGO cathode for high-rate and long-life sodium-ion batteries. *Small Methods* 2021;5:e2100372. DOI

38. Yuan T, Wang Y, Zhang J, et al. 3D graphene decorated $Na_4Fe_3(PO_4)_2(P_2O_7)$ microspheres as low-cost and high-performance cathode materials for sodium-ion batteries. *Nano Energy* 2019;56:160-8. DOI

39. Pu X, Wang H, Yuan T, et al. $Na_4Fe_3(PO_4)_2P_2O_7$/C nanospheres as low-cost, high-performance cathode material for sodium-ion batteries. *Energy Stor Mater* 2019;22:330-6. DOI

40. Sharma L, Adiga SP, Alshareef HN, Barpanda P. Fluorophosphates: next generation cathode materials for rechargeable batteries. *Adv Energy Mater* 2020;10:2001449. DOI

41. Reddy M, Subba Rao G, Chowdari B. Long-term cycling studies on 4V-cathode, lithium vanadium fluorophosphate. *J Power Sources* 2010;195:5768-74. DOI

42. Ellis BL, Ramesh TN, Davis LJ, Goward GR, Nazar LF. Structure and electrochemistry of two-electron redox couples in lithium metal fluorophosphates based on the tavorite structure. *Chem Mater* 2011;23:5138-48. DOI

43. Recham N, Chotard J, Jumas J, Laffont L, Armand M, Tarascon J. Ionothermal synthesis of Li-based fluorophosphates electrodes. *Chem Mater* 2010;22:1142-8. DOI

44. Prabu M, Reddy M, Selvasekarapandian S, Rao GS, Chowdari B. Synthesis, impedance and electrochemical studies of lithium iron fluorophosphate, $LiFePO_4F$ cathode. *Electrochim Acta* 2012;85:572-8. DOI

45. Rangaswamy P, Suresh GS, Mahadevan MK. Comprehensive electrochemical studies of tavorite $LiTiPO_4F$/C electrode for rechargeable lithium ion battery. *Chem Select* 2016;1:1472-83. DOI

46. Nagahama M, Hasegawa N, Okada S. High voltage performances of Li_2NiPO_4F cathode with dinitrile-based electrolytes. *J Electrochem Soc* 2010;157:A748. DOI

47. Wang D, Xiao J, Xu W, et al. Preparation and electrochemical investigation of Li_2CoPO_4F cathode material for lithium-ion batteries. *J Power Sources* 2011;196:2241-5. DOI

48. Amaresh S, Karthikeyan K, Kim K, et al. Facile synthesis of ZrO_2 coated Li_2CoPO_4F cathode materials for lithium secondary batteries with improved electrochemical properties. *J Power Sources* 2013;244:395-402. DOI

49. Xu M, Cheng CJ, Sun QQ, et al. A 3D porous interconnected $NaVPO_4F$/C network: preparation and performance for Na-ion batteries. *RSC Adv* 2015;5:40065-9. DOI

50. Recham N, Chotard J, Dupont L, Djellab K, Armand M, Tarascon J. Ionothermal synthesis of sodium-based fluorophosphate cathode materials. *J Electrochem Soc* 2009;156:A993. DOI

51. Pu X, Wang H, Zhao D, et al. Recent progress in rechargeable sodium-ion batteries: toward high-power applications. *Small* 2019;15:e1805427. DOI

52. Zou H, Li S, Wu X, Mcdonald MJ, Yang Y. Spray-drying synthesis of pure Na_2CoPO_4F as cathode material for sodium ion batteries. *ECS Electrochem Lett* 2015;4:A53. DOI

53. Wu L, Hu Y, Zhang X, Liu J, Zhu X, Zhong S. Synthesis of carbon-coated Na_2MnPO_4F hollow spheres as a potential cathode material for Na-ion batteries. *J Power Sources* 2018;374:40-7. DOI

54. Hu F, Jiang X. Superior performance of carbon modified $Na_3V_2(PO_4)_2F_3$ cathode material for sodium-ion batteries. *Inorg Chem Commun* 2021;129:108653. DOI

55. Gover R, Bryan A, Burns P, Barker J. The electrochemical insertion properties of sodium vanadium fluorophosphate, $Na_3V_2(PO_4)_2F_3$. *Solid State Ion* 2006;177:1495-500. DOI

56. Law M, Balaya P. NaVPO4F with high cycling stability as a promising cathode for sodium-ion battery. *Energy Stor Mater* 2018;10:102-13. DOI

57. Fang Y, Xiao L, Chen Z, Ai X, Cao Y, Yang H. Recent advances in sodium-ion battery materials. *Electrochem Energy Rev* 2018;1:294-323. DOI

58. Wu J, Xu Y, Sun X, Wang C, Zhang B, Zhao J. The multiple effects of potassium doping on LiVPO4F/C composite cathode material for lithium ion batteries. *J Power Sources* 2018;396:155-63. DOI

59. Ati M, Sathiya M, Boulineau S, et al. Understanding and promoting the rapid preparation of the triplite-phase of LiFeSO4F for use as a large-potential Fe cathode. *J Am Chem Soc* 2012;134:18380-7. DOI

60. Tripathi R, Gardiner GR, Islam MS, Nazar LF. Alkali-ion conduction paths in LiFeSO4F and NaFeSO4F tavorite-type cathode materials. *Chem Mater* 2011;23:2278-84. DOI

61. Recham N, Chotard JN, Dupont L, et al. A 3.6 V lithium-based fluorosulphate insertion positive electrode for lithium-ion batteries. *Nat Mater* 2010;9:68-74. DOI

62. Kim M, Kim D, Lee W, Jang HM, Kang B. New class of 3.7 V Fe-based positive electrode materials for Na-ion battery based on cation-disordered polyanion framework. *Chem Mater* 2018;30:6346-52. DOI

63. Barpanda P, Chotard JN, Recham N, et al. Structural, transport, and electrochemical investigation of novel $AMSO_4F$ (A = Na, Li; M = Fe, Co, Ni, Mn) metal fluorosulphates prepared using low temperature synthesis routes. *Inorg Chem* 2010;49:7401-13. DOI

64. Heo J, Jung S, Hwang I, et al. Amorphous iron fluorosulfate as a high-capacity cathode utilizing combined intercalation and conversion reactions with unexpectedly high reversibility. *Nat Energy* 2023;8:30-9. DOI

65. Lu W, Xie K, Chen Z, Xiong S, Pan Y, Zheng C. A new co-solvent for wide temperature lithium ion battery electrolytes: 2,2,2-Trifluoroethyl n-caproate. *J Power Sources* 2015;274:676-84. DOI

66. Yang Y, Li P, Wang N, et al. Fluorinated carboxylate ester-based electrolyte for lithium ion batteries operated at low temperature. *Chem Commun* 2020;56:9640-3. DOI

67. Hess S, Wohlfahrt-mehrens M, Wachtler M. Flammability of Li-ion battery electrolytes: flash point and self-extinguishing time measurements. *J Electrochem Soc* 2015;162:A3084. DOI

68. Shiga T, Kato Y, Kondo H, Okuda C. Self-extinguishing electrolytes using fluorinated alkyl phosphates for lithium batteries. *J Mater Chem A* 2017;5:5156-62. DOI

69. Chen L, Shen X, Chen H, et al. High-stable nonflammable electrolyte regulated by coordination-number rule for all-climate and safer lithium-ion batteries. *Energy Stor Mater* 2023;55:836-46. DOI

70. He M, Su C, Feng Z, et al. High voltage $LiNi_{0.5}Mn_{0.3}Co_{0.2}O_2$/graphite cell cycled at 4.6 V with a FEC/HFDEC-based electrolyte. *Adv Energy Mater* 2017;7:1700109. DOI

71. Lu W, Xie K, Chen ZX, Pan Y, Zheng CM. Preparation and characterization of trifluoroethyl aliphatic carboxylates as co-solvents for the carbonate-based electrolyte of lithium-ion batteries. *J Fluorine Chem* 2014;161:110-9. DOI

72. Fan X, Chen L, Ji X, et al. Highly fluorinated interphases enable high-voltage Li-metal batteries. *Chem* 2018;4:174-85. DOI

73. Luo Y, Lu T, Zhang Y, Yan L, Xie J, Mao SS. Enhanced electrochemical performance of $LiNi_{0.5}Mn_{1.5}O_4$ cathode using an electrolyte with 3-(1,1,2,2-tetrafluoroethoxy)-1,1,2,2-tetrafluoropropane. *J Power Sources* 2016;323:134-41. DOI

74. Gu W, Xue G, Dong Q, et al. Trimethoxyboroxine as an electrolyte additive to enhance the 4.5 V cycling performance of a Ni-rich layered oxide cathode. *eScience* 2022;2:486-93. DOI

75. He Z, Chen Y, Huang F, et al. Fluorinated Solvents for lithium metal batteries. *Acta Phys Chim Sin* 2022;38:2205005. DOI

76. Chen J, Fan X, Li Q, et al. Electrolyte design for LiF-rich solid-electrolyte interfaces to enable high-performance microsized alloy anodes for batteries. *Nat Energy* 2020;5:386-97. DOI

77. Chen L, Wu H, Ai X, Cao Y, Chen Z. Toward wide-temperature electrolyte for lithium-ion batteries. *Battery Energy* 2022;1:20210006. DOI

78. Lu W, Xie K, Pan Y, Chen Z, Zheng C. Effects of carbon-chain length of trifluoroacetate co-solvents for lithium-ion battery electrolytes using at low temperature. *J Fluor Chem* 2013;156:136-43. DOI

79. Liu Y, Zheng L, Gu W, Shen Y, Chen L. Surface passivation of lithium metal via *in situ* polymerization. *Acta Physico Chimica Sinica* 2021;37:2004058. DOI

80. Ma X, Yu J, Hu Y, Texter J, Yan F. Ionic liquid/poly(ionic liquid)-based electrolytes for lithium batteries. *Ind Chem Mater* 2023;1:39-59. DOI

81. Goodenough JB, Kim Y. Challenges for rechargeable Li batteries. *Chem Mater* 2010;22:587-603. DOI

82. Choudhury S, Archer LA. Lithium fluoride additives for stable cycling of lithium batteries at high current densities. *Adv Elect Mater* 2016;2:1500246. DOI

83. Zhang XQ, Chen X, Xu R, et al. Columnar lithium metal anodes. *Angew Chem Int Ed* 2017;56:14207-11. DOI

84. Zhao J, Liao L, Shi F, et al. Surface fluorination of reactive battery anode materials for enhanced stability. *J Am Chem Soc* 2017;139:11550-8. DOI

85. Lee J, Kim YJ, Jin HS, et al. Tuning two interfaces with fluoroethylene carbonate electrolytes for high-performance Li/LCO batteries.

ACS Omega 2019;4:3220-7. DOI PubMed PMC

86.   Zhang XQ, Cheng XB, Chen X, Yan C, Zhang Q. Fluoroethylene carbonate additives to render uniform Li deposits in lithium metal batteries. *Adv Funct Mater* 2017;27:1605989. DOI

87.   Chen Y, Dong C, Chen L, et al. "One stone two birds" design for hollow spherical $Na_4Fe_3(PO_4)_2P_2O_7$/C cathode enabled high-performance sodium-ion batteries from iron rust. *EcoMat* 2023;5:e12393. DOI

88.   Wen Y, Wang B, Luo B, Wang L. Long-term cycling performance of nitrogen-doped hollow carbon nanospheres as anode materials for sodium-ion batteries. *Eur J Inorg Chem* 2016;2016:2051-5. DOI

89.   Veith GM, Doucet M, Sacci RL, Vacaliuc B, Baldwin JK, Browning JF. Determination of the solid electrolyte interphase structure grown on a silicon electrode using a fluoroethylene carbonate additive. *Sci Rep* 2017;7:6326. DOI PubMed PMC

90.   Choi N, Yew KH, Lee KY, Sung M, Kim H, Kim S. Effect of fluoroethylene carbonate additive on interfacial properties of silicon thin-film electrode. *J Power Sources* 2006;161:1254-9. DOI

91.   He M, Guo R, Hobold GM, Gao H, Gallant BM. The intrinsic behavior of lithium fluoride in solid electrolyte interphases on lithium. *Proc Natl Acad Sci USA* 2020;117:73-9. DOI PubMed PMC

92.   Miao R, Yang J, Feng X, Jia H, Wang J, Nuli Y. Novel dual-salts electrolyte solution for dendrite-free lithium-metal based rechargeable batteries with high cycle reversibility. *J Power Sources* 2014;271:291-7. DOI

93.   Yang G, Li Y, Liu S, Zhang S, Wang Z, Chen L. LiFSI to improve lithium deposition in carbonate electrolyte. *Energy Stor Mater* 2019;23:350-7. DOI

94.   Yamada Y, Wang J, Ko S, Watanabe E, Yamada A. Advances and issues in developing salt-concentrated battery electrolytes. *Nat Energy* 2019;4:269-80. DOI

95.   Wang J, Yamada Y, Sodeyama K, et al. Fire-extinguishing organic electrolytes for safe batteries. *Nat Energy* 2018;3:22-9. DOI

96.   Piao N, Ji X, Xu H, et al. Countersolvent electrolytes for lithium-metal batteries. *Adv Energy Mater* 2020;10:1903568. DOI